AAPS PharmSciTech, Vol. 14, No. 2, June 2013 (© 2013)
DOI: 10.1208/s12249-013-9936-2

Research Article

The Effect of Nonideal Cascade Impactor Stage Collection Efficiency Curves on the Interpretation of the Size of Inhaler-Generated Aerosols

D. L. Roberts[1] and J. P. Mitchell[2,3]

Received 9 October 2012; accepted 29 January 2013; published online 19 March 2013

Abstract. Cascade impactors, operating on the principle of inertial size separation in (ideally) laminar flow, are used to determine aerodynamic particle size distributions (APSDs) of orally inhaled product (OIP) aerosols because aerodynamic diameter can be related to respiratory tract deposition. Each stage is assumed typically to be an ideal size fractionator. Thus, all particles larger than a certain size are considered collected and all finer particles are treated as penetrating to the next stage (a step function stage efficiency curve). In reality, the collection efficiency of a stage smoothly increases with particle size as an "S-shaped" curve, from approximately 0% to 100%. Consequently, in some cases substantial overlap occurs between neighboring stages. The potential for bias associated with the step-function assumption has been explored, taking full resolution and two-stage abbreviated forms of the Andersen eight-stage nonviable impactor (ACI) and the next-generation pharmaceutical impactor (NGI) as example apparatuses. The behavior of unimodal, log-normal APSDs typical of OIP-generated aerosols has been investigated, comparing known input values to calculated values of central tendency (mass median aerodynamic diameter) and spread (geometric standard deviation, GSD). These calculations show that the error introduced by the step change assumption is larger for the ACI than for the NGI. However, the error is sufficiently small to be inconsequential unless the APSD in nearly monodisperse (GSD ≤1.2), a condition that is unlikely to occur with realistic OIPs. Account may need to be taken of this source of bias only for the most accurate work with abbreviated ACI systems.

KEY WORDS: cascade impactor; inhaler aerosol; inhaler testing; size distribution.

INTRODUCTION

Cascade impactors (CIs) operate on the principle of inertial size-separation in laminar flow (1). They are widely used to determine aerodynamic particle size distributions (APSDs) of orally inhaled product (OIP) aerosols because aerodynamic size can be related to particle deposition in the respiratory tract (2). Furthermore, the mass of active pharmaceutical ingredient (API) can be recovered from a CI and assayed quantitatively in a fully traceable manner (3). The European and US pharmacopeial methods for APSD assessment (4,5) describe specific CIs including the widely used Andersen eight-stage nonviable impactor (ACI) and the next-generation pharmaceutical impactor (NGI). Regulatory agency guidance documents relating to the *in vitro* testing of OIPs cite the use of cascade impaction as the norm for the aerodynamic particle size assessment of emitted aerosols (6–8).

The function of a multistage CI is primarily to fractionate the incoming aerosol into groups possessing progressively finer sizes, beginning with the coarsest particles (1,9,10). The linear air velocity is increased in a series of well-defined steps as the aerosol particles move from one stage to the next in the apparatus, in order to achieve this outcome. These increases are put into effect primarily by reductions in the nozzle diameter from one stage to the next in the series. However, the number of nozzles per stage (N) as well as the number of stages within the CI (n) can also be adjusted to optimize size resolution and minimize pressure drop across especially the stages that size separate the finest subfractions (9,10).

The raw data from a CI comprise the mass of collected particles on each stage. The simplest relationship of the mass on a stage to the aerodynamic size appropriate to that component of the CI can be derived by assuming that the stage of interest captures all particles larger than a given size with 100% efficiency and all particles smaller than this given size with 0% efficiency. In this model, where the collection efficiency changes immediately from 0% to 100%, the cut-point size is traditionally defined where the *actual* stage efficiency is 50% (known as D_{50} or the cut-point size; dashed line in Fig. 1). The value of D_{50} can be calculated from the particle Stokes number (St) which is a dimensionless quantity derived from the equations of motion of a particle in laminar flow in a circular jet directed perpendicular to a flat surface. Marple

Electronic supplementary material The online version of this article (doi:10.1208/s12249-013-9936-2) contains supplementary material, which is available to authorized users.

[1] MSP Corporation, St. Paul, Minnesota, USA.
[2] Trudell Medical International, 725 Third Street, London, Ontario, Canada N5V 5G4.
[3] To whom correspondence should be addressed. (e-mail: jmitchell@trudellmed.com)

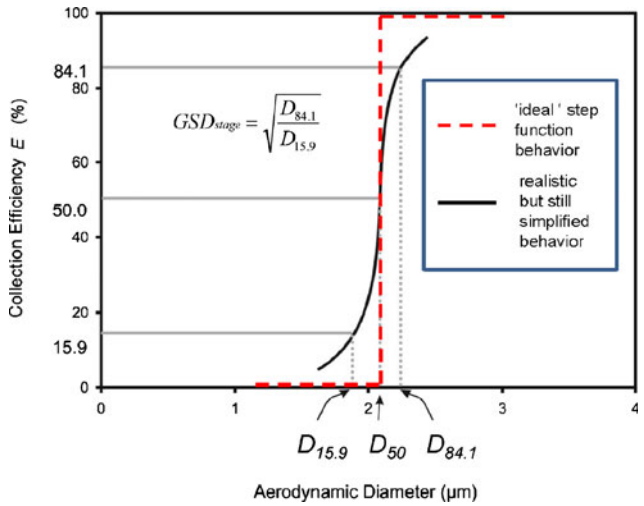

Fig. 1. CI stage collection efficiency curve showing "ideal" step function case and realistic but simplified model for establishing cut size (D_{50}) and related measures ($D_{15.9}$ and $D_{84.1}$), used to describe the sharpness of cut for the stage

and Liu (9) showed from a theoretical assessment of laminar flow in a model CI that $\sqrt{St_{50}}$ is always close to 0.49 for nozzles having circular exit profiles, in accordance with the relationship defined by Eq. 1 at volumetric flow rate, Q:

$$\sqrt{C_{50}}D_{50} = \left[\frac{9\pi\mu NW^3}{4\rho_0 Q}\right]^{\frac{1}{2}}\sqrt{St_{50}} \qquad (1)$$

Here, W is the nozzle diameter of the array containing "N" separate nozzles, all of which are assumed to have the same diameter. The other parameters relate to the Cunningham slip correction term (C_{50}), air viscosity (μ), unit density (cgs system; ρ_0), all of which are constants for particular measurement conditions.

In reality, the collection efficiency of a given stage (E_{stage}) is a smooth function of aerodynamic diameter (solid line in Fig. 1), transitioning from its minimum to maximum values about the aerodynamic size at which the stage is 50% efficient (D_{50} value). This function is often assumed to possess symmetry about D_{50}, meaning that the mass of particles larger than this size penetrating the stage in question, is exactly compensated by the mass associated with particles that are finer but which are collected thereon (*N.B.* this assumption cannot be true in general but could be true in some specific cases). With this assumption, the D_{50} for a given stage can still be defined as a single-valued constant for operation of the CI at a fixed flow rate. This simplification avoids the need to invoke mass-per-stage data inversion measures that would require the shape of the response function for each stage of the CI to be defined mathematically (11). By analogy with the properties of a unimodal and log-normal distribution, the "spread" of a real collection efficiency curve is often defined as the geometric standard deviation of the stage (GSD_{stage}). GSD_{stage} is the square root of the ratio of the sizes $D_{84.1}$ and $D_{15.9}$, at which E_{stage} corresponds to 84.1% and 15.9%, respectively (Fig. 1). GSD_{stage} is unity for an ideal stage (dashed line in Fig. 1), but in practice this measure of stage size selectivity is <1.3 for all stages of a well-designed CI (3). If a mathematically rigorous approach is adopted, the stage response (or kernel function), can be defined as the fraction of particles entering the impactor that are collected on the ith stage. The ith stage response is obtained as the product of its efficiency ($E_{stage(i)}$), and terms describing the fraction of particles reaching the ith stage (i.e., the fraction that is neither lost to the internal walls nor collected on previous stages (12)). On the other hand, if, as was mentioned earlier, the choice is made to simplify the data analysis process by reducing each real stage collection efficiency curve of a multistage CI to a single value based on its D_{50} value, a further assumption is tacitly made that there is negligible overlap between collection efficiency curves of adjacent stages (13). This supposition is not entirely true with current CI designs (13), as significant stage overlap may occur, especially at the extremes of the collection efficiency curves (E_{stage}<15% or E_{stage}>85%). Such behavior is clearly evident in the calibration data (Fig. 2) obtained with monodisperse particles of known aerodynamic diameter for designs such as the ACI (14). Although it is not possible to be certain, in retrospect, it appears that attention was not paid during the design of this CI to space the individual stage D_{50} values uniformly as a function of aerodynamic size scaled logarithmically. However, the more recently developed NGI was intentionally designed with sharp individual stage collection efficiency profiles that are equally spaced on the logarithmically scaled aerodynamic diameter axis, so as to minimize stage overlap. At the same time, five stages for APSD resolution in the critical range from 0.5- to 5.0-μm aerodynamic diameter are available throughout almost all of its operating flow rate range from 30 to 100 L/min for the assessment of pressurized metered dose (pMDI) and dry powder inhalers (15). Stage overlap, if ignored, has the potential to introduce unexpected outcomes when comparing full-resolution CI data to equivalent measurements from abbreviated impactors derived from the same "parent" CI (16). The presence of significant adjacent stage overlap is important because the removal of intermediate stages is almost certain to eliminate such superimposition, thereby modifying the intermediate particle size distribution that is presented to the succeeding stage of the abbreviated system, compared with the situation that exists with the full-resolution CI.

The purpose of this investigation was to explore theoretically how the assumption of an ideal step-function change in collection efficiency from 0% to 100% at the D_{50} size might

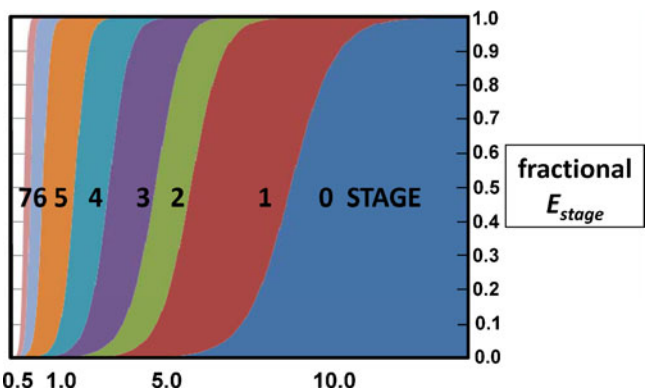

Fig. 2. Stage collection efficiency profiles for the ACI at 28.3 L/min; note the significant overlap between certain stages, in particular stages 2 and 3

affect the accuracy of measured APSD-derived data for two CIs (the ACI and NGI). These CIs are the most widely encountered apparatuses for OIP aerosol assessments, based on a survey of European Pharmaceutical Aerosol Group members conducted in 2005 (17) and repeated in 2012 (18). Each system was "challenged" with an array of input model aerosols that were defined as having unimodal and log-normal APSDs so that their mass median aerodynamic diameter (MMAD) and GSD values could be specified unambiguously. It is acknowledged that the APSDs of many OIP-generated aerosols do not fully meet this criterion (19). Nevertheless, the assumption that OIP aerosols can be treated as unimodal and log-normally distributed, is believed to be a fair approximation to the actual situation, particularly those generated by pMDIs (20), which is why the compendial methods also make this assumption in relation to APSD data analysis (4,5).

Given the interest in reducing the number of size-fractionating stages in either apparatus to as few as two, as part of the AIM concept (16), the investigation was extended to examine how measurements made by two particular abbreviated impactor configurations of significant interest as potential AIM apparatuses (both based on the same "parent" full-resolution CI) might be influenced by idealized data interpretation methods. This part of the study involved comparisons of full-resolution CI to AIM-derived APSD metrics, i.e., coarse, fine and extra-fine mass, with common, and appropriate size limits defined to be pertinent to the size-classification of OIP-generated aerosols.

Methods: Full-Resolution CIs

The flow diagram (Fig. 3) illustrates the concept underlying this part of the investigation. An *n*-stage CI (either the NGI or ACI) was challenged with a series of incoming aerosols whose size properties ($MMAD_{input}$ and GSD_{input}) encompassed the ranges from 1.1 to 5.0 µm and from 1.2 to 2.2, respectively. The full stage-efficiency curves defined for the ACI at 28.3 L/min and for the NGI at 30 L/min were applied to interpret how each incoming aerosol is size fractionated, because each set of profiles provide exact descriptions of how the particle mass (m_1 ....m_n) is distributed within the CI in question. The exact expression for the fraction of the mass that deposits on stage "*n*" is given by Eq. 2:

$$f_n = \frac{1}{\sqrt{2\pi}}\frac{1}{\ell n\sigma_g}\cdot\int_0^{\infty}\frac{1}{x}\exp\left[-\frac{1}{2}\frac{(\ell nx-\ell n\overline{D})^2}{(\ell n\sigma_g)^2}\right]\cdot E_n(x)[(1-E_0(x))\cdot(1-E_1(x))....(1-E_{n-1}(x))]dx \quad (2)$$

Here, σ_g is the geometric standard deviation (GSD_{input}), and $\overline{D}$ is identical with $MMAD_{input}$. The quantities E_0 … E_n are the fractional collection efficiency curves of stages *0* to *n* of the multistage CI (E_0 is set to zero for the NGI because there is no stage designated as "zero" for this CI).

$MMAD_{calc}$ and GSD_{calc} were calculated as defined in the pharmacopeial compendia (4,5), with these actual masses on each stage taken as "data." These moments of the APSD were also calculated using CITDAS® CI data analysis software (Copley Scientific Ltd., Nottingham, UK), which is widely employed in OIP assessments and which assumes linearity of selected near-neighbor points on a log-probit plot of the cumulative mass-weighted APSD (21). These "linear" curve-fit calculations, based on a log-normal-scaled APSD, assume that input aerosol is unimodal and that the particles collecting on each stage are all smaller than the D_{50} value of the stage immediately above.

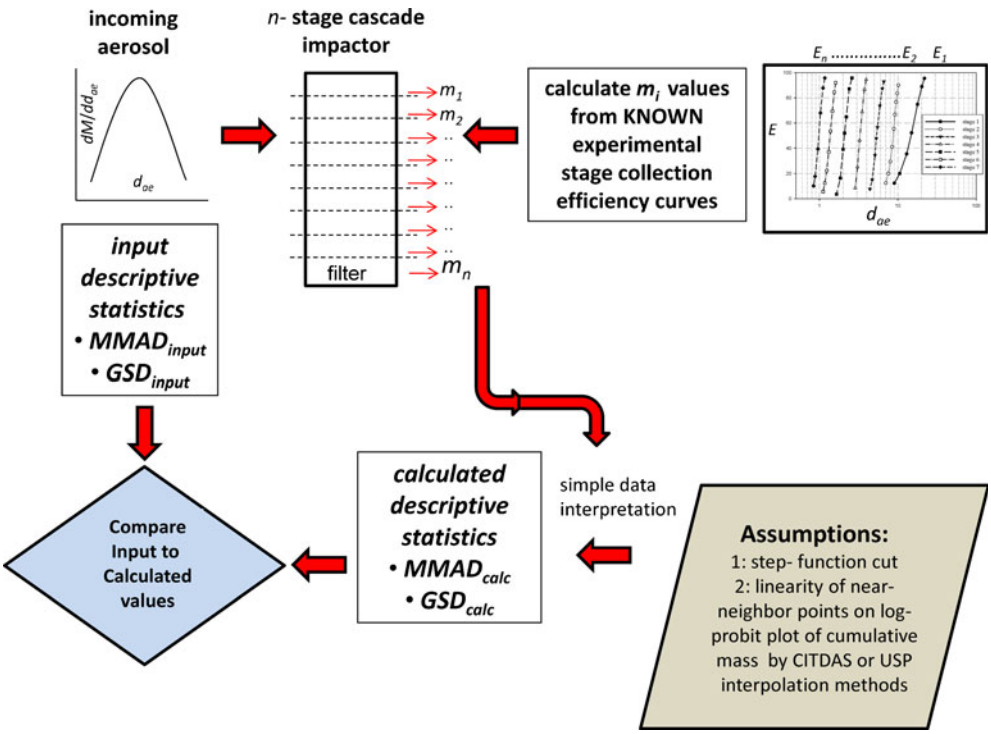

Fig. 3. Process flow diagram for assessment of full-resolution CIs with model input aerosols; these aerosols were assumed to have unimodal and log-normal APSDs

Rader *et al.* (12) have shown that CI stage efficiency curves can each be described accurately in analytic form using the hyperbolic tangent function:

$$E_i(d_{pc}) = \tanh\left[\left(\frac{d_{pc}}{Y_i}\right)^{Z_i}\right] \quad (3)$$

in which d_{pc} is the modified particle diameter corrected for slip in accordance with the expression:

$$d_{pc} = d_p\sqrt{\frac{\rho_p}{\rho_0}}\sqrt{C_{dp}} = d_{ae}\sqrt{C(d_{ae})} \quad (4)$$

C_{dp} is the Cunningham slip correction factor associated with the physical diameter of the particle, d_p (22), and Y_i and Z_i are best fit parameters for each impaction stage. More recently, Roberts derived values of Y_i and Z_i for the NGI (23) based on the stage collection-efficiency curves from the archival calibration of this CI undertaken at four different flow rates (24,25). These values are summarized in Table I for operation at the flow rate of 30 L/min considered in the present study, chosen so as to allow comparison to the ACI, for which complete collection efficiency curves for all stages at 28.3 L/min are available in the public domain (14). The size-selectivity of the stage collection efficiency curves for the NGI at 30 L/min was deemed as illustrative of the stage collection efficiency curve sharpness throughout its operating range, as equivalent curves at 15, 60, and 100 L/min have been shown to be comparable in shape (24,25) but displaced in terms of D_{50} values in accordance with Eq. 1. Inasmuch as archival calibration data are at present unavailable for the ACI, the exponential function developed by Gulak *et al.* (26) was used to define the stage efficiency curves at 28.3 L/min for this CI:

$$E_i(d_{ae}) = \frac{1}{1+\exp(A_i d_{ae} + B_i)} \quad (5)$$

This particular flow rate was chosen as it is specified for pMDI assessments in the pharmacopeias (3,4), and therefore widely used. Table I also lists the values of the parameters A_i and B_i that best fitted the calibration data of Vaughan (14) at 28.3 L/min, which are frequently cited as being representative for this CI. However, the D_{50} size for stage 2 was chosen to be 4.7-μm aerodynamic diameter, in keeping with the current pharmacopeial specification for this apparatus, rather than 5.7-μm aerodynamic diameter, as reported by Vaughan (14).

Using either Eqs. 3 or 4 depending on CI type, Eq. 2 was evaluated numerically via Simpson's Rule (27), with the particle size span set from 0.01 to 21 μm in increments of 0.01 μm. All calculations were undertaken using EXCEL* (version 14.0.5128.5000; 2010, Microsoft Corporation, Redmond, WA).

The fraction of the input aerosol mass that actually lies between size D_n and D_{n-1} can be determined analytically by setting the $E_i(x)$ functions in Eq. 2 equal to step functions at the values of D_{50} for the stages:

$$f_n = \frac{1}{2}\left\{erf\left[\frac{\ell n\left(\frac{D_{50,n-1}}{\bar{D}}\right)}{\sqrt{2}\ell n(\sigma_g)}\right] - erf\left[\frac{\ell n\left(\frac{D_{50,n}}{\bar{D}}\right)}{\sqrt{2}\ell n(\sigma_g)}\right]\right\} \quad (6)$$

The error function (erf(x)) given by Eqs. 3–54 in Matthews and Walker (27) was used to evaluate Eq. 6:

$$erf(x) = \frac{2}{\sqrt{\pi}}\int_0^x \exp(-h^2)dh \quad (7)$$

in which "h" is the variable of integration. At the inlet of the impactor, particles can be any size, and so the value of $D_{50,\ n-1}$ was set to infinity for the incoming aerosol entering the CI from the induction port (note that erf(∞)=1). Hence, Eq. 6 allowed comparison of the mass fractions collected on each stage (as computed by Eq. 2) to the actual mass in a given size range in the inlet aerosol.

Method: Abbreviated CIs

Abbreviation of either of the two full-resolution CI systems involved regarding most of the stages as being rendered non-operational. In the case of the abbreviated NGI, it was postulated that the user removed the air flow after stage 3 and reintroduced it just upstream of stage 6 making use of special cups that are available for the NGI (MSP Corporation; see Svensson and Berg (28)). In this arrangement, the abbreviated NGI behaves much like a full-resolution NGI but with fewer stages (Fig. 4a). In the case of the ACI, the user was assumed to have retained only stages 2, 5, and the back-up filter stages (Fig. 4b), as described for the "Trudell" Fast Screening Andersen impactor (T-FSA) by Mitchell *et al.* (29). Note that the spacer stage shown for the T-FSA, located above the first stage (stage 2), played no part in the present analysis, as it is used to obtain comparable dead-space so that formulations containing low volatile solvents, such as ethanol, have similar evaporation behavior to that in the full-resolution ACI (30).

Table I. Stage Collection Efficiency Curve Parameters for NGI and ACI Operated at 30 and 28.3 L/min, Respectively

Parameter (Eq. 3)	NGI stage number[a]							
	1	2	3	4	5	6	7	
Y_i	14.06357	7.17380	4.51830	2.55956	1.53432	0.97550	0.65988	
Z_i	3.79914	6.48198	5.64470	9.00492	9.99737	7.85323	9.04608	
Parameter (Eq. 5)	ACI stage number							
	0	1	2	3	4	5	6	7
A_i	−1.324	−1.874	−1.928	−2.808	−4.494	−8.258	−14.82	−17.76
B_i	12.51	11.39	9.604	9.329	9.668	8.787	9.483	7.725

[a] More significant digits are provided than justified by experimental precision, so as to avoid rounding errors

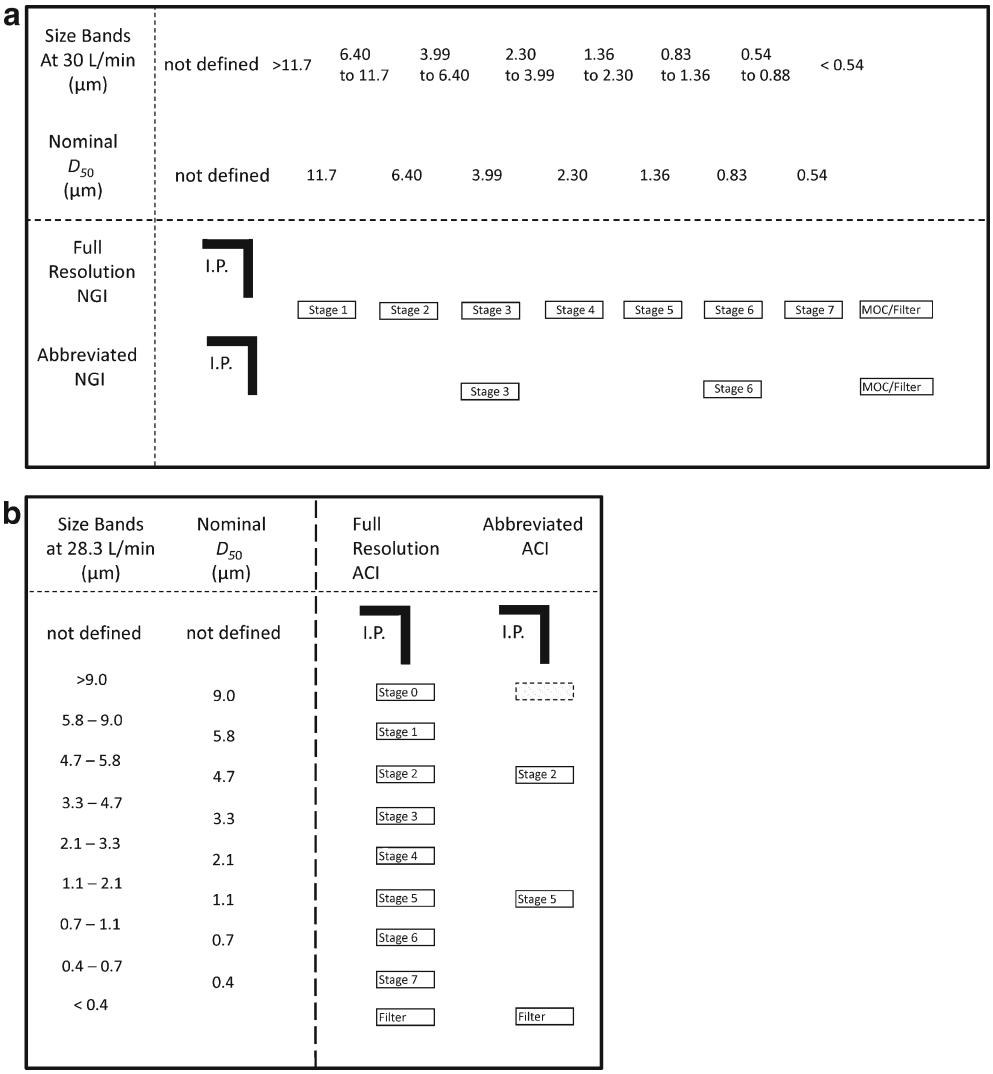

Fig. 4. Abbreviated impactors compared with their full-resolution counterparts (IP=USP/Ph. Eur. induction port): **a** NGI and **b** ACI

A similar approach to that described for the full-resolution CIs was undertaken to assess theoretically the performance for two configurations that were deemed representative of options that are likely to be of importance if the AIM concept is applied to OIP aerosol measurements (Fig. 5). Values of mass of extra-fine ($M_{ef–abb}$), fine ($M_{f–abb}$), and coarse ($M_{c–abb}$) particles that actually distributed in each abbreviated CI configuration were calculated using the stage efficiency curves for the corresponding reduced impactor. The stage efficiency functions, $E_i(x)$, in Eq. 2 were set equal to zero for stages of the full-resolution stages that were removed, and therefore the same equation for the mass fraction on a stage obtains as for the full-resolution impactor:

$$f_n = \frac{1}{\sqrt{2\pi}} \frac{1}{\ell n \sigma_g} \cdot \int_0^\infty \frac{1}{x} \exp\left[-\frac{1}{2} \frac{\left(\ell nx - \ell n\overline{D}\right)^2}{\left(\ell n \sigma_g\right)^2}\right] \cdot E_n(x) \times [(1 - E_0(x))(1 - E_1(x))....(1 - E_{n-1}(x))]dx \quad (8)$$

Equation 8 was evaluated for the abbreviated impactors numerically with Simpson's rule (31), just as for the full-resolution impactors. The resulting mass on each stage of the abbreviated impactor was compared with the relevant value of mass ($M_{ef–full}$, $M_{f–full}$, and $M_{c–full}$) from the summed stages of the appropriate full-resolution CI (Eq. 2). And finally, these calculated values of mass assigned to each stage of the abbreviated CI could be compared with the actual mass in the relevant size range of the inlet aerosol via Eq. 6.

RESULTS AND DISCUSSION

Calculated mass-per-stage data are tabulated in parts I and II of the Electronic Supplementary Material for the NGI and ACI, respectively, where they are compared with the input aerosol mass distributed within the given size range for the stage in question. Tables II and III of the main article contain the magnitudes of the errors associated with calculated values of $MMAD_{CI}$ and GSD_{CI} for each input APSD presented to the NGI and ACI, respectively. These errors are each expressed as a percentage of its corresponding $MMAD_{input}$ or GSD_{input} value.

The magnitude of the deviations in APSD central tendency, reported as $MMAD_{CI}$, associated with the use of real rather than ideal stage collection efficiency curves were

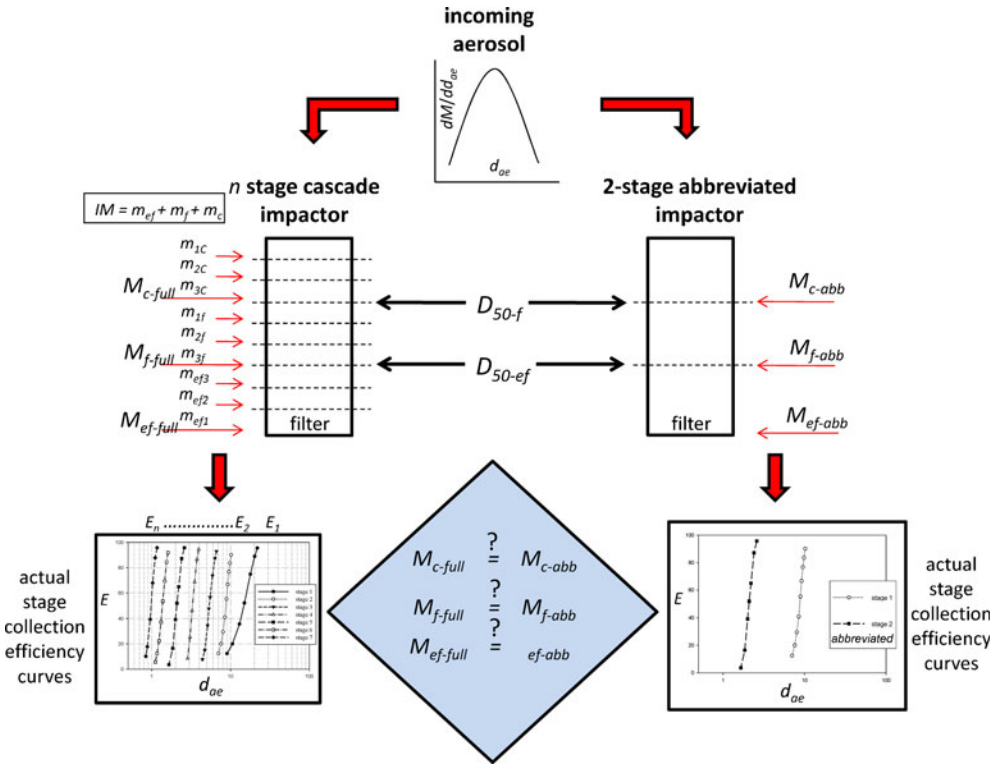

Fig. 5. Process flow diagram for assessment of two abbreviated CIs with model input aerosols; these aerosols were assumed to have unimodal and log-normal APSDs

similar for the two CIs, ranging between +4.8% and −3.0% for the NGI and from +5.5% to −7.6% for the ACI, respectively. The corresponding ranges for GSD_{CI} exceeded 10% in a few cases, varying from +11.7% to 0.0% for the NGI and from +10.8% to −5.0% for the ACI. There were no marked trends associated with either CI type or input APSD characteristics. However, as a general rule, making the assumption of ideal stage collection curves in most instances resulted in only minor broadening of the output APSD combined with correspondingly small shifts of $MMAD_{CI}$ to larger sizes. The increased deviations in GSD_{CI} that were most noticeable with aerosols having the smallest GSD_{input} of 1.2 was anticipated, since the size-fractionation of such near-to-monodisperse aerosols, regardless of their MMAD, is intuitively more sensitive to the precise shape of the stage collection efficiency profiles of the one or two stages in the CI *at most*, at which size-fractionation takes place to a significant extent (32). Taken to an extreme, it follows that size fractionation of a hypothetical near-to-perfectly monodisperse aerosol (GSD_{input}=1.01) by a single ideal stage in the CI whose collection efficiency profile is a step function at its D_{50} size will depend critically on the magnitude of the difference between $MMAD_{input}$ and the D_{50} value of the stage in question.

Fortuitously, currently marketed OIP-generated aerosols are polydisperse, almost all having *MMAD* values in the range 1 to 5 μm (comparable with the range of input values examined here), and with corresponding values of GSD that lie mostly in the range from 1.8 to 2.2 (20,33). It therefore follows that the error introduced by assuming that the stage collection efficiency profiles can be represented by their D_{50} values alone is expected to be small, regardless whether the NGI or ACI is used as the measurement apparatus. The example shown in Fig. 6 illustrates this finding more clearly. The model APSD having $MMAD_{input}$ and GSD_{input} of 5.0 μm and 2.2 respectively was intentionally chosen for this illustration since the overlap between the collection efficiency profiles for stages 2 and 3 of the ACI occurring at ca. 5 μm aerodynamic diameter is most apparent (Fig. 2). Returning to Fig. 6, an

Table II. Calculated Error Magnitudes Expressed as Percentages of the Corresponding Input APSD for the Full-Resolution NGI

	GSD_{input}									
	1.2		1.5		1.6		2.0		2.2	
$MMAD_{input}$ (μm)	$MMAD_{CI}$	GSD_{CI}	$MMAD_{CI}$	GSD_{CI}	$MMAD_{CI}$	GSD_{CI}	$MMAD_{CI}$	GSD_{CI}	$MMAD_{CI}$	GSD_{CI}
1.1	+1.8	+4.2	+1.8	+2.7	+2.7	+1.9	0.0	0.0	+2.7	+2.3
2.5	+4.8	+10.8	+3.2	+6.7	+3.2	+5.6	+2.8	+4.0	+2.4	+3.2
4.0	+3.3	+11.1	+4.3	+4.7	+4.3	+5.6	+3.0	+3.5	+1.0	+0.9
5.0	+3.4	+11.7	+3.8	+10.0	+3.6	+8.8	+0.4	+3.0	−3.0	+0.5

Table III. Calculated Error Magnitudes Expressed as Percentages of the Corresponding Input APSD for the Full-Resolution ACI

	GSD_{input}									
	1.2		1.5		1.6		2.0		2.2	
$MMAD_{input}$ (μm)	$MMAD_{CI}$	GSD_{CI}	$MMAD_{CI}$	GSD_{CI}	$MMAD_{CI}$	GSD_{CI}	$MMAD_{CI}$	GSD_{CI}	$MMAD_{CI}$	GSD_{CI}
1.1	+4.5	+10.8	+5.5	+2.0	+5.5	+0.6	+5.5	−1.0	+5.5	−0.9
2.5	+1.2	+10.0	+1.2	+4.0	+1.2	+3.1	+1.2	−0.5	+0.8	−2.3
4.0	−0.5	+5.0	0.0	0.0	+0.3	−0.6	−1.0	−3.5	−3.0	−5.0
5.0	−2.6	+5.8	−2.0	+1.3	−2.0	+0.6	−4.6	−2.0	−7.6	+7.3

error band representing 5% deviation either side of the input APSD is also shown to give perspective to these calculated deviations. It is self-evident that the calculated NGI-based APSD was very close to that of the input aerosol whereas the calculated APSD for the ACI was shifted slightly further to finer sizes, mostly as a result of the significant overlap between its stage 2 and stages 1 and 3. However, APSDs deduced by idealized data interpretation methods with either CI were within the error band.

When examining the effect of abbreviating a given CI, it is necessary to examine how these changes in APSD moments caused by assuming ideal stage collection behavior that have already been described translate into measures that are more directly pertinent to the mass of active pharmaceutical ingredient contained in size ranges that are linked (however tenuously) to regions of particle deposition in the human respiratory tract (34,35). For the purposes of this article, three such regions were therefore defined as follows:

1. Coarse fraction; (M_c), largely depositing in the oro- or naso-pharynx (34), defined by NGI stages 1–3 (d_{ae}> 3.99 μm) or ACI stages 0–2 (d_{ae}>4.7 μm);
2. Fine fraction; (M_f), most likely to deposit in the airways of the lungs (34), defined by NGI stages 4–6 (0.83<d_{ae}<3.99 μm) or ACI stages 3–5 (1.1<d_{ae}<4.7 μm);
3. Extra-fine fraction; (M_{ef}), most likely either to deposit in the alveolar spaces and associated distal airways (36), or to be exhaled (37), defined by NGI stages 7-MOC/filter (d_{ae}< 0.83 μm) or ACI stages 6-filter (d_{ae}<1.1 μm).

Comparisons between the mass derived from the input APSD and the corresponding mass calculated assuming actual stage collection efficiency profiles (arbitrary units) on each of the grouped stages of the NGI and ACI are summarized in the first two columns under the heading "calculated deposition" in Tables IV and V, respectively. Both tables also contain the corresponding values for abbreviated NGI and ACI configurations in which the remaining stages were selected such that their D_{50} values matched with each full-resolution CI stage grouping (compare Fig. 4a, b).

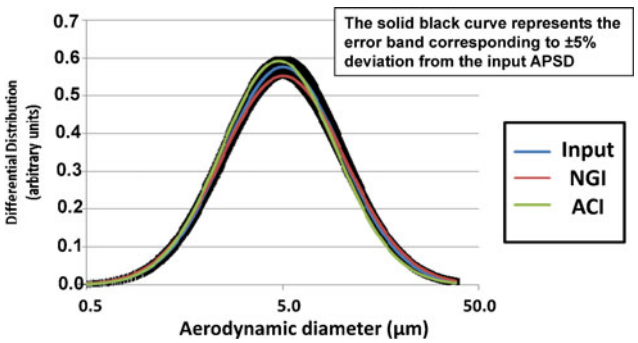

Fig. 6. Input and calculated APSDs from hypothetical OIP-generated aerosol having values of $MMAD_{input}$ and GSD_{input} of 5 μm and 2.0, respectively; the *error band* represents a 5% deviation about the input aerosol APSD

The absolute values (Δm) of the deviations between the calculated deposited mass in each abbreviated CI configuration ($m_{component}$) and the corresponding values from the input APSD (m_{input}) covering the same size range were compared with the mass that would have been apportioned based on the size characteristics of the input aerosol APSD, in accordance with:

$$\Delta m = m_{component} - m_{input} \tag{9}$$

The subscript "*component*" represents the selected stage grouping for consideration. These values are summarized in Tables VI and VII for the NGI and ACI systems, respectively. No bias due to the assumption of ideal stage collection efficiency behavior is indicated where Δm=0.

The full-resolution CI would normally be considered as the reference apparatus in method development for an abbreviated apparatus. In order to compare how the deviations associated with the abbreviated CIs matched with their corresponding full-resolution "parent" apparatus, Eq. 9 was modified to the form:

$$\Delta m = \sum_{i-m}^{i-n} m_{grouped-stages} - m_{input} \tag{10}$$

The sum of the mass collecting on stages m to n, represents the grouped stage mass for each full-resolution CI configuration, calculated according to the same size range criteria established above. These results are also summarized in Tables VI and VII for the NGI and ACI configurations, respectively.

In Tables VI and VII, the sensitivity of Δm to divergence between ideal and actual stage collection efficiency profiles is maximized where the magnitude of the apportioned mass to a given stage grouping for the full-resolution systems or stage number in the case of the abbreviated impactors is greatest. However, normalizing to the magnitude of mass assigned to each location based on the input APSD would have resulted in values of infinity in cases where the input aerosol apportioned mass was zero. Notwithstanding this

Table IV. Comparison between Calculated Measures of Deposited Mass in Abbreviated and Full-Resolution NGI Apparatuses for Selected Input APSDs Representative of OIP Aerosols

$APSD_{input}$					Calculated deposition (arbitrary units of mass)		
$MMAD_{input}$	GSD_{input}	Size range (μm)	Grouped mass descriptor	Stage number at boundary size[a]	Input aerosol	Grouped stages from NGI	Mass on each stage of abbreviated NGI
1.1	1.2	>3.99	M_c	1–3	0.0000	0.0009	0.0008
		0.83–3.99	M_f	4–6	0.9358	0.9160	0.9155
		<0.83	M_{ef}	7-MOC/filter	0.0642	0.0830	0.0837
	1.5	>3.99	M_c	1–3	0.0007	0.0055	0.0052
		0.83–3.99	M_f	4–6	0.7522	0.7617	0.7614
		<0.83	M_{ef}	7-MOC/filter	0.2470	0.2328	0.2334
	1.6	>3.99	M_c	1–3	0.0031	0.0102	0.0096
		0.83–3.99	M_f	4–6	0.7193	0.7287	0.7286
		<0.83	M_{ef}	7 MOC/filter	0.2776	0.2611	0.2617
	2.0	>3.99	M_c	1–3	0.0316	0.0445	0.0434
		0.83–3.99	M_f	4–6	0.6239	0.6279	0.6286
		<0.83	M_{ef}	7-MOC/filter	0.3446	0.3275	0.3280
	2.2	>3.99	M_c	1–3	0.0512	0.0650	0.0636
		0.83–3.99	M_f	4–6	0.5863	0.5886	0.5896
		<0.83	M_{ef}	7-MOC/filter	0.3626	0.3464	0.3468
2.5	1.2	>3.99	M_c	1–3	0.0052	0.0721	0.0683
		0.83–3.99	M_f	4–6	0.9948	0.9279	0.9317
		<0.83	M_{ef}	7-MOC/filter	0.0000	0.0000	0.0000
	1.5	>3.99	M_c	1–3	0.1247	0.1767	0.1720
		0.83–3.99	M_f	4–6	0.8719	0.8195	0.8241
		<0.83	M_{ef}	7-MOC/filter	0.0034	0.0039	0.0039
	1.6	>3.99	M_c	1–3	0.1602	0.2055	0.2009
		0.83–3.99	M_f	4–6	0.8301	0.7844	0.7889
		<0.83	M_{ef}	7-MOC/filter	0.0097	0.0101	0.0102
	2.0	>3.99	M_c	1–3	0.2502	0.2794	0.2756
		0.83–3.99	M_f	4–6	0.6932	0.6654	0.6691
		<0.83	M_{ef}	7-MOC/filter	0.0565	0.0552	0.0553
	2.2	>3.99	M_c	1–3	0.2768	0.2997	0.2962
		0.83–3.99	M_f	4–6	0.6414	0.6188	0.6221
		<0.83	M_{ef}	7-MOC/filter	0.0818	0.0815	0.0816
4.0	1.2	>3.99	M_c	1–3	0.5065	0.5477	0.5361
		0.83–3.99	M_f	4–6	0.4935	0.4523	0.4639
		<0.83	M_{ef}	7-MOC/filter	0.0000	0.0000	0.0000
	1.5	>3.99	M_c	1–3	0.5029	0.5386	0.5318
		0.83–3.99	M_f	4–6	0.4970	0.4613	0.4681
		<0.83	M_{ef}	7-MOC/filter	0.0001	0.0001	0.0001
	1.6	>3.99	M_c	1–3	0.5025	0.5352	0.5292
		0.83–3.99	M_f	4–6	0.4970	0.4641	0.4701
		<0.83	M_{ef}	7-MOC/filter	0.0004	0.0007	0.0007
	2.0	>3.99	M_c	1–3	0.5017	0.5185	0.5141
		0.83–3.99	M_f	4–6	0.4864	0.4616	0.4659
		<0.83	M_{ef}	7-MOC/filter	0.0118	0.0199	0.0200
	2.2	>3.99	M_c	1–3	0.5015	0.5065	0.5026
		0.83–3.99	M_f	4–6	0.4751	0.4534	0.4572
		<0.83	M_{ef}	7-MOC/filter	0.0234	0.0402	0.0402
5.0	1.2	>3.99	M_c	1–3	0.8926	0.8510	0.8441
		0.83–3.99	M_f	4–6	0.1074	0.1490	0.1559
		<0.83	M_{ef}	7-MOC/filter	0.0000	0.0000	0.0000
	1.5	>3.99	M_c	1–3	0.7115	0.7247	0.7191
		0.83–3.99	M_f	4–6	0.2885	0.2751	0.2807
		<0.83	M_{ef}	7-MOC/filter	0.0000	0.0002	0.0002
	1.6	>3.99	M_c	1–3	0.6848	0.7005	0.6954
		0.83–3.99	M_f	4–6	0.3151	0.2982	0.3034
		<0.83	M_{ef}	7-MOC/filter	0.0001	0.0012	0.0012
	2.0	>3.99	M_c	1–3	0.6279	0.6276	0.6237
		0.83–3.99	M_f	4–6	0.3672	0.3483	0.3523
		<0.83	M_{ef}	7-MOC/filter	0.0049	0.0240	0.0241
	2.2	>3.99	M_c	1–3	0.6129	0.5968	0.5932
		0.83–3.99	M_f	4–6	0.3756	0.3577	0.3612
		<0.83	M_{ef}	7-MOC/filter	0.0115	0.0455	0.0456

[a] Based on full-resolution NGI

Table V. Comparison Between Calculated Measures of Deposited Mass in Abbreviated and Full-Resolution ACI Apparatuses for Selected Input APSDs Representative of OIP Aerosols

$APSD_{input}$					Calculated deposition (arbitrary units of mass)		
$MMAD_{input}$	GSD_{input}	Size range (μm)	Grouped mass descriptor	Stage number at boundary size[a]	Input aerosol	Grouped stages from ACI	Mass on each stage of abbreviated ACI
1.1	1.2	>4.7	M_c	2	0.0000	0.0008	0.0006
		1.1–4.7	M_f	5	0.5000	0.5653	0.5618
		<1.1	M_{ef}	Filter	0.5000	0.4339	0.4376
	1.5	>4.7	M_c	2	0.0002	0.0018	0.0016
		1.1–4.7	M_f	5	0.4998	0.5438	0.5415
		<1.1	M_{ef}	Filter	0.5000	0.4543	0.4569
	1.6	>4.7	M_c	2	0.0010	0.0034	0.0030
		1.1–4.7	M_f	5	0.4990	0.5381	0.5361
		<1.1	M_{ef}	Filter	0.5000	0.4586	0.4609
	2.0	>4.7	M_c	2	0.0181	0.0221	0.0203
		1.1–4.7	M_f	5	0.4819	0.5089	0.5089
		<1.1	M_{ef}	Filter	0.5000	0.4690	0.4708
	2.2	>4.7	M_c	2	0.0327	0.0365	0.0340
		1.1–4.7	M_f	5	0.4673	0.4913	0.4921
		<1.1	M_{ef}	Filter	0.5000	0.4722	0.4738
2.5	1.2	>4.7	M_c	2	0.0003	0.0162	0.0141
		1.1–4.7	M_f	5	0.9997	0.9834	0.9854
		<1.1	M_{ef}	Filter	0.0000	0.0004	0.0005
	1.5	>4.7	M_c	2	0.0597	0.0773	0.0701
		1.1–4.7	M_f	5	0.9188	0.8968	0.9035
		<1.1	M_{ef}	Filter	0.0214	0.0259	0.0264
	1.6	>4.7	M_c	2	0.0896	0.1034	0.0950
		1.1–4.7	M_f	5	0.8700	0.8536	0.8614
		<1.1	M_{ef}	Filter	0.0403	0.0431	0.0436
	2.0	>4.7	M_c	2	0.1812	0.1850	0.1750
		1.1–4.7	M_f	5	0.7007	0.7014	0.7105
		<1.1	M_{ef}	Filter	0.1181	0.1136	0.1144
	2.2	>4.7	M_c	2	0.2117	0.2111	0.2012
		1.1–4.7	M_f	5	0.6395	0.6446	0.6535
		<1.1	M_{ef}	Filter	0.1489	0.1444	0.1452
4.0	1.2	>4.7	M_c	2	0.1882	0.2359	0.2114
		1.1–4.7	M_f	5	0.8118	0.7641	0.7886
		<1.1	M_{ef}	Filter	0.0000	0.0000	0.0000
	1.5	>4.7	M_c	2	0.3454	0.3458	0.3238
		1.1–4.7	M_f	5	0.6539	0.6528	0.6747
		<1.1	M_{ef}	Filter	0.0007	0.0014	0.0014
	1.6	>4.7	M_c	2	0.3658	0.3640	0.3437
		1.1–4.7	M_f	5	0.6312	0.6317	0.6519
		<1.1	M_{ef}	Filter	0.0030	0.0043	0.0044
	2.0	>4.7	M_c	2	0.4080	0.3964	0.3810
		1.1–4.7	M_f	5	0.5607	0.5641	0.5793
		<1.1	M_{ef}	Filter	0.0313	0.0394	0.0397
	2.2	>4.7	M_c	2	0.4190	0.3981	0.3841
		1.1–4.7	M_f	5	0.5303	0.5352	0.5487
		<1.1	M_{ef}	Filter	0.0508	0.0668	0.0672
5.0	1.2	>4.7	M_c	2	0.5178	0.5619	0.6328
		1.1–4.7	M_f	5	0.4822	0.4381	0.3672
		<1.1	M_{ef}	Filter	0.0000	0.0000	0.0000
	1.5	>4.7	M_c	2	0.5155	0.5418	0.5606
		1.1–4.7	M_f	5	0.4841	0.4578	0.4393
		<1.1	M_{ef}	Filter	0.0004	0.0004	0.0001
	1.6	>4.7	M_c	2	0.5134	0.5367	0.5524
		1.1–4.7	M_f	5	0.4844	0.4612	0.4470
		<1.1	M_{ef}	Filter	0.0022	0.0021	0.0006
	2.0	>4.7	M_c	2	0.5356	0.5087	0.4921
		1.1–4.7	M_f	5	0.4500	0.4574	0.4737
		<1.1	M_{ef}	Filter	0.0145	0.0340	0.0342
	2.2	>4.7	M_c	2	0.5313	0.4906	0.4759
		1.1–4.7	M_f	5	0.4413	0.4482	0.4626
		<1.1	M_{ef}	Filter	0.0274	0.0613	0.0615

[a] Based on full-resolution ACI

Table VI. Deviations Between Calculated Deposited Mass in Abbreviated and Grouped Stages of Full-Resolution NGI Operating Within Same Size Range and Corresponding Values of Input Aerosol Mass Partitioned Between Ideal Stages

$APSD_{input}$					Deviation from input aerosol (M_{full}–M_{abb}; arbitrary units of mass)		
$MMAD_{input}$	GSD_{input}	Size range (μm)	Grouped mass descriptor	Full resolution CI stage numbers	Grouped stages from NGI	Mass on each stage of abbreviated NGI	Abbreviated CI stage numbers
1.1	1.2	>3.99	M_c	1–3	+0.0009	+0.0008	1
		0.83–3.99	M_f	4–6	−0.0198	−0.0203	2
		<0.83	M_{ef}	7-MOC/filter	+0.0188	+0.0195	Filter
	1.5	>3.99	M_c	1–3	+0.0048	+0.0045	1
		0.83–3.99	M_f	4–6	+0.0095	+0.0092	2
		<0.83	M_{ef}	7-MOC/filter	−0.0142	−0.0136	Filter
	1.6	>3.99	M_c	1–3	+0.0071	+0.0065	1
		0.83–3.99	M_f	4–6	+0.0094	+0.0093	2
		<0.83	M_{ef}	7-MOC/filter	−0.0165	−0.0159	Filter
	2.0	>3.99	M_c	1–3	+0.0129	+0.0118	1
		0.83–3.99	M_f	4–6	+0.0040	+0.0047	2
		<0.83	M_{ef}	7-MOC/filter	−0.0171	−0.0166	Filter
	2.2	>3.99	M_c	1–3	+0.0138	+0.0124	1
		0.83–3.99	M_f	4–6	+0.0023	+0.0033	2
		<0.83	M_{ef}	7-MOC/filter	−0.0162	−0.0158	Filter
2.5	1.2	>3.99	M_c	1–3	+0.0669	+0.0631	1
		0.83–3.99	M_f	4–6	−0.0669	−0.0631	2
		<0.83	M_{ef}	7-MOC/filter	0.0000	0.0000	Filter
	1.5	>3.99	M_c	1–3	+0.0520	+0.0473	1
		0.83–3.99	M_f	4–6	−0.0524	−0.0478	2
		<0.83	M_{ef}	7-MOC/filter	+0.0004	+0.0005	Filter
	1.6	>3.99	M_c	1–3	+0.0453	+0.0407	1
		0.83–3.99	M_f	4–6	−0.0457	0.0412	2
		<0.83	M_{ef}	7-MOC/filter	+0.0004	+0.0005	filter
	2.0	>3.99	M_c	1–3	+0.0292	+0.0254	1
		0.83–3.99	M_f	4–6	−0.0278	−0.0241	2
		<0.83	M_{ef}	7-MOC/filter	−0.0013	−0.0012	Filter
	2.2	>3.99	M_c	1–3	+0.0229	+0.0194	1
		0.83–3.99	M_f	4–6	−0.0226	−0.0193	2
		<0.83	M_{ef}	7-MOC/filter	−0.0003	−0.0002	Filter
4.0	1.2	>3.99	M_c	1–3	+0.0412	+0.0296	1
		0.83–3.99	M_f	4–6	−0.0412	−0.0296	2
		<0.83	M_{ef}	7-MOC/filter	0.0000	0.0000	Filter
	1.5	>3.99	M_c	1–3	+0.0357	+0.0289	1
		0.83–3.99	M_f	4–6	−0.0357	−0.0289	2
		<0.83	M_{ef}	7-MOC/filter	0.0000	0.0000	Filter
	1.6	>3.99	M_c	1–3	+0.0327	+0.0267	1
		0.83–3.99	M_f	4–6	−0.0329	−0.0269	2
		<0.83	M_{ef}	7-MOC/filter	+0.0003	+0.0003	Filter
	2.0	>3.99	M_c	1–3	+0.0168	+0.0124	1
		0.83–3.99	M_f	4–6	−0.0248	−0.0205	2
		<0.83	M_{ef}	7-MOC/filter	+0.0081	+0.0082	Filter
	2.2	>3.99	M_c	1–3	+0.0050	+0.0011	1
		0.83–3.99	M_f	4–6	−0.0217	−0.0179	2
		<0.83	M_{ef}	7-MOC/filter	+0.0168	+0.0168	Filter
5.0	1.2	>3.99	M_c	1–3	−0.0416	−0.0485	1
		0.83–3.99	M_f	4–6	+0.0416	+0.0485	2
		<0.83	M_{ef}	7-MOC/filter	0.0000	0.0000	Filter
	1.5	>3.99	M_c	1–3	+0.0132	+0.0076	1
		0.83–3.99	M_f	4–6	−0.0134	−0.0078	2
		<0.83	M_{ef}	7-MOC/filter	+0.0002	+0.0002	Filter
	1.6	>3.99	M_c	1–3	+0.0157	+0.0106	1
		0.83–3.99	M_f	4–6	−0.0169	−0.0117	2
		<0.83	M_{ef}	7-MOC/filter	+0.0011	+0.0011	Filter
	2.0	>3.99	M_c	1–3	−0.0003	−0.0042	1
		0.83–3.99	M_f	4–6	−0.0189	−0.0149	2
		<0.83	M_{ef}	7-MOC/filter	+0.0191	+0.0192	Filter
	2.2	>3.99	M_c	1–3	−0.0161	−0.0197	1
		0.83–3.99	M_f	4–6	−0.0179	−0.0144	2
		<0.83	M_{ef}	7-MOC/filter	+0.0340	+0.0341	Filter

Table VII. Deviations Between Calculated Deposited Mass in Abbreviated and Grouped Stages of Full-Resolution ACI Operating Within Same Size Range and Corresponding Values of Input Aerosol Mass Partitioned Between Ideal Stages

$APSD_{input}$					Calculated deposition (arbitrary units of mass)		
$MMAD_{input}$	GSD_{input}	Size range (μm)	Grouped mass descriptor	Stage number	Grouped stages from ACI	Mass on each stage of abbreviated ACI	Abbreviated CI stage numbers
1.1	1.2	>4.7	M_c	0–2	+0.0008	+0.0006	1
		1.1–4.7	M_f	3–5	+0.0653	+0.0618	2
		<1.1	M_{ef}	6-filter	−0.0661	−0.0624	Filter
	1.5	>4.7	M_c	0–2	+0.0016	+0.0014	1
		1.1–4.7	M_f	3–5	+0.0440	+0.0417	2
		<1.1	M_{ef}	6-filter	−0.0457	−0.0431	Filter
	1.6	>4.7	M_c	0–2	+0.0024	+0.0020	1
		1.1–4.7	M_f	3–5	+0.0391	+0.0371	2
		<1.1	M_{ef}	6-filter	−0.0414	−0.0391	Filter
	2.0	>4.7	M_c	0–2	+0.0040	+0.0022	1
		1.1–4.7	M_f	3–5	+0.0270	+0.0270	2
		<1.1	M_{ef}	6-filter	−0.0310	−0.0292	Filter
	2.2	>4.7	M_c	0–2	+0.0038	+0.0013	1
		1.1–4.7	M_f	3–5	+0.0240	+0.0248	2
		<1.1	M_{ef}	6-filter	−0.0278	−0.0262	Filter
2.5	1.2	>4.7	M_c	0–2	+0.0159	+0.0138	1
		1.1–4.7	M_f	3–5	−0.0163	−0.0143	2
		<1.1	M_{ef}	6-filter	+0.0004	+0.0005	Filter
	1.5	>4.7	M_c	0–2	+0.0176	+0.0104	1
		1.1–4.7	M_f	3–5	−0.0220	−0.0153	2
		<1.1	M_{ef}	6-filter	+0.0045	+0.0050	Filter
	1.6	>4.7	M_c	0–2	+0.0138	+0.0054	1
		1.1–4.7	M_f	3–5	−0.0164	−0.0086	2
		<1.1	M_{ef}	6-filter	+0.0028	+0.0033	Filter
	2.0	>4.7	M_c	0–2	+0.0038	−0.0062	1
		1.1–4.7	M_f	3–5	+0.0007	+0.0098	2
		<1.1	M_{ef}	6-filter	−0.0045	−0.0037	Filter
	2.2	>4.7	M_c	0–2	−0.0006	−0.0105	1
		1.1–4.7	M_f	3–5	+0.0051	+0.0140	2
		<1.1	M_{ef}	6-filter	−0.0045	−0.0037	Filter
4.0	1.2	>4.7	M_c	0–2	+0.0477	+0.0232	1
		1.1–4.7	M_f	5	−0.0477	−0.0232	2
		<1.1	M_{ef}	Filter	0.0000	0.0000	Filter
	1.5	>4.7	M_c	0–2	+0.0004	−0.0216	1
		1.1–4.7	M_f	3–5	−0.0011	+0.0208	2
		<1.1	M_{ef}	6-filter	+0.0007	+0.0007	Filter
	1.6	>4.7	M_c	0–2	−0.0018	−0.0221	1
		1.1–4.7	M_f	3–5	+0.0005	+0.0207	2
		<1.1	M_{ef}	6-filter	+0.0013	+0.0014	Filter
	2.0	>4.7	M_c	0–2	−0.0116	−0.0270	1
		1.1–4.7	M_f	3–5	+0.0034	+0.0186	2
		<1.1	M_{ef}	6-filter	+0.0081	+0.0084	Filter
	2.2	>4.7	M_c	0–2	−0.0209	−0.0349	1
		1.1–4.7	M_f	3–5	+0.0049	+0.0184	2
		<1.1	M_{ef}	6-filter	+0.0160	+0.0164	Filter
5.0	1.2	>4.7	M_c	0–2	+0.0441	+0.1150	1
		1.1–4.7	M_f	5	−0.0441	−0.1150	2
		<1.1	M_{ef}	Filter	0.0000	0.0000	Filter
	1.5	>4.7	M_c	0–2	+0.0263	+0.0451	1
		1.1–4.7	M_f	3–5	−0.0263	−0.0448	2
		<1.1	M_{ef}	6-filter	0.0000	−0.0003	Filter
	1.6	>4.7	M_c	0–2	+0.0233	+0.0390	1
		1.1–4.7	M_f	3–5	−0.0233	−0.0374	2
		<1.1	M_{ef}	6-filter	−0.0001	−0.0016	Filter
	2.0	>4.7	M_c	0–2	−0.0269	−0.0435	1
		1.1–4.7	M_f	3–5	+0.0074	+0.0237	2
		<1.1	M_{ef}	6-filter	+0.0195	+0.0197	Filter
	2.2	>4.7	M_c	0–2	−0.0407	−0.0554	1
		1.1–4.7	M_f	3–5	+0.0069	+0.0213	2
		<1.1	M_{ef}	6-filter	+0.0339	+0.0341	Filter

limitation, it is possible to make some observations of a general nature:

1. Values of Δm obtained with each stage of the appropriate abbreviated apparatus (NGI or ACI) tracked those associated with the corresponding grouped stage of the parent full-resolution CI;
2. For a given MMAD, the largest values of Δm associated with a particular stage grouping or abbreviated CI stage number were generally associated with input APSDs whose *GSD*s were nearest to being monodisperse (i.e., at 1.2), this behavior was most evident where $MMAD_{input}$ was relatively large (4.0 or 5.0 μm);
3. The relative magnitude of Δm associated with a particular stage grouping or abbreviated CI stage number was greater for the ACI than the NGI where $MMAD_{input}$ was at its finest (1.1 μm), otherwise these measures were comparable.

If it is assumed that the mass of aerosol associated with fine particles (M_f) represents the most beneficial portion of the emitted dose from the majority of currently marketed OIPs that are intended for therapy in relation to obstructive and inflammatory lung diseases (37), it is instructive to compare the ratios of the calculated values of this metric associated with the abbreviated impactors (R_f), in accordance with:

$$R_f = \frac{M_{f(abb)}}{M_{f(full)}} \tag{11}$$

Again using in each case, the corresponding values from grouped stages of the corresponding full-resolution systems as the reference condition. R_f is 100% when there is perfect concordance between measures obtained by abbreviated and full-resolution CI configurations. Bias introduced by abbreviating either the NGI or ACI was small (Figs. 7a (NGI) and 8a (ACI)), generally increasing with relatively large $MMAD_{input}$ combined with decreased GSD_{input}. For the abbreviated NGI, in the worst case, R_f deviated by +4.4% from perfect concordance, where the input aerosol characteristics were $MMAD_{input}$=5.0 μm and GSD_{input}=1.2. Similar but more pronounced trends with $MMAD_{input}$ and GSD_{input} were observed for the abbreviated ACI; for this system, in the worst case, R_f deviated by −9.9% from perfect concordance, where the input aerosol characteristics were also $MMAD_{input}$=5.0 μm and GSD_{input}=1.2. This outcome would be

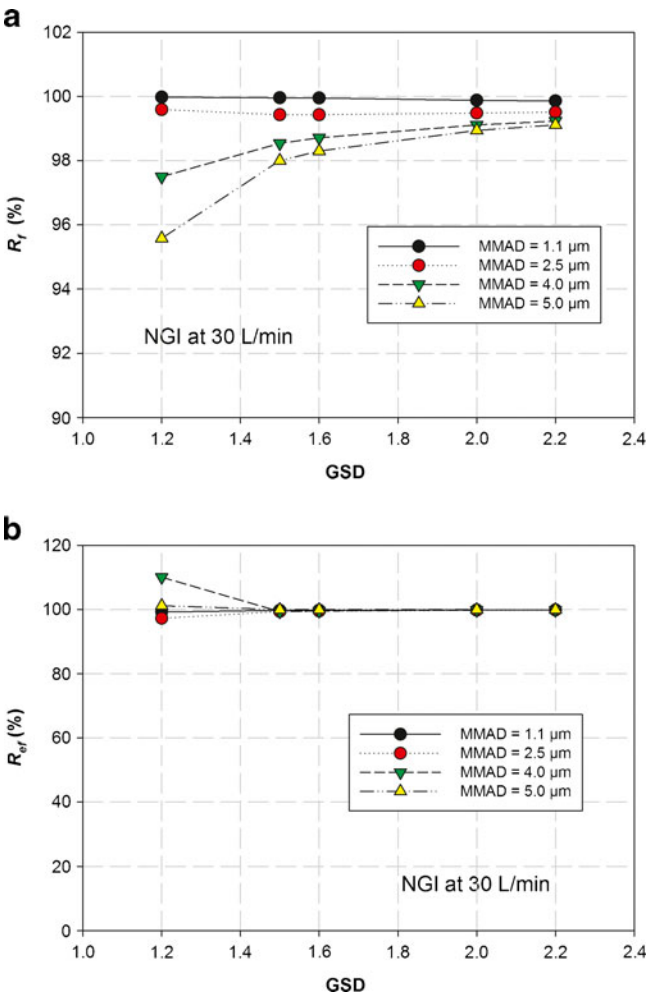

Fig. 7. Deviations in the ratios of fine (R_f) and extra-fine (R_{ef}) particle fraction from unimodal log-normal input APSDs for NGI operated at 30 L/min

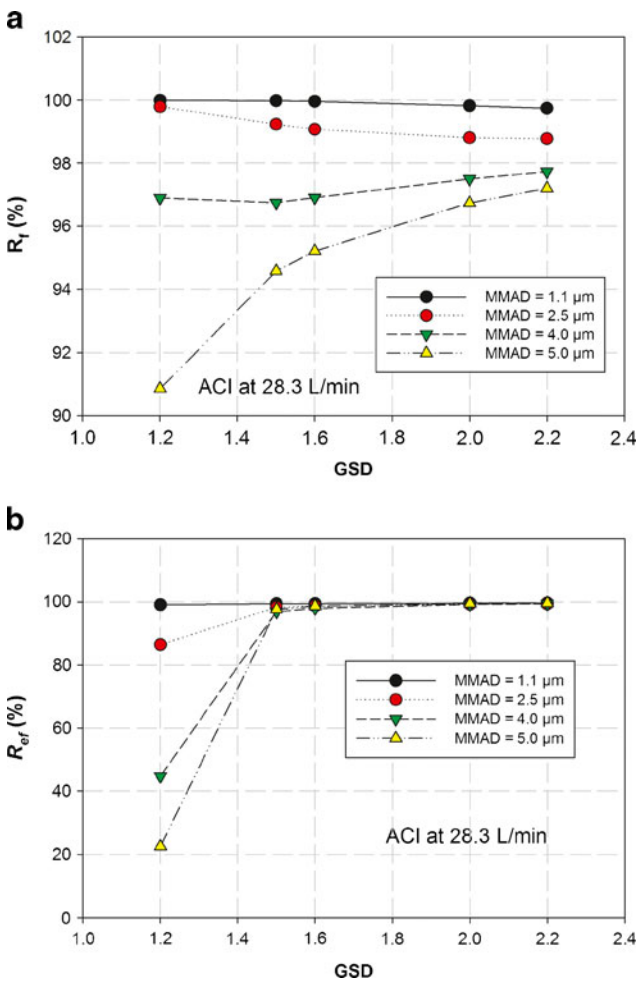

Fig. 8. Deviations in the ratios of fine (R_f) and extra-fine (R_{ef}) particle fraction from unimodal log-normal input APSDs for ACI operated at 28.3 L/min

consistent with removal in the abbreviated system of the significant overlap that exists between the collection efficiency curves for stage 2 and adjacent stages with this particular full-resolution CI. By eliminating overlap, the remaining stage of the abbreviated ACI configuration is presented with a different incoming intermediate size distribution containing additional larger particles that would have been captured by the preceding stages that are present in the full-resolution configuration. This modified intermediate particle size distribution is then less effectively captured by the abbreviated ACI. Given the present findings, it is likely that bias associated with this effect will be small enough to be inconsequential for currently marketed OIP characterization. However, it may be of concern, should a near-to monodisperse product become available whose GSD is <1.5. In contrast, the reduced stage efficiency curve overlap associated with the NGI (24,25), it is considered unlikely that the discrepancies in values of R_f (all<4.5%) would be observable experimentally, given the magnitude of other contributors to the overall variability of the CI method (38).

It is also a useful exercise to examine the behavior of the mass apportioned to the extra-fine particles ≤1.1 μm, given their potential importance for distal airway and alveolar delivery (37). The same approach as described for calculating R_f was therefore used to determine the ratio for extra-fine particle mass (R_{ef}) since, by analogy with Eq. 11:

$$R_{ef} = \frac{M_{ef(abb)}}{M_{ef(full)}} \tag{12}$$

The potential for bias to R_{ef} to be introduced by abbreviating either the NGI or ACI was in most instances small and comparable with the corresponding values of R_f for a given input APSD (Figs. 7b (NGI) and 8b (ACI)). In the worst case with the NGI ($MMAD_{input}$=4.0 μm; GSD_{input}=1.2), this bias attained a value that was close to +10%. In contrast, however, the corresponding bias associated with the ACI for input aerosols having GSD values of 1.2 was as much as −77.4% for the case in which $MMAD_{input}$ was 5.0 μm and was <10% only for the case where $MMAD_{input}$ was 1.1 μm. Interestingly, bias predicted for the abbreviated ACI was much smaller, being <4% regardless of $MMAD_{input}$, when GSD_{input} was >1.2. For the NGI, the potential for bias in measures of R_{ef} associated with abbreviating the system are deemed likely to be inconsequential, except perhaps for highly monodisperse aerosols. However, although bias associated with R_{ef} for an abbreviated ACI appears to be sufficiently small that it can be ignored for OIP-generated polydisperse aerosols, such a system would likely be unusable in comparison with its full-resolution ACI, should a monodisperse product become available.

CONCLUSIONS

This theoretical study simulated the inertial size fractionation of well-characterized aerosols in terms of their MMAD and GSD values by the NGI and ACI, two widely used CIs for the assessment of OIPs. These apparatuses imperfectly separate incoming aerosol into subfractions, because the collection efficiency of each stage is not an ideal step function from zero to 100%. This nonideal size separation of the CI stages can be properly accounted for by considering the actual capture efficiency of each stage, in order to obtain a more accurate understanding of the input aerosol APSD, based on the real properties of the CI stages. The size distribution properties for the several input aerosols were chosen to be typical of those produced by many OIPs. The evidence from these comparisons is that the impact of idealized data interpretation methods will have a minimal influence on the understanding of the input aerosol APSDs when such calculations are undertaken, irrespective of CI type. This finding most probably arises because of the symmetry of each collection efficiency curve about its D_{50} size. Thus the mass of API assumed to be captured by a given stage, when not the case in actuality is almost compensated for by the mass assumed to pass the stage but that is actually captured there. It is therefore concluded that there is no need for this refinement in calculating APSDs using either of these full-resolution CIs.

Abbreviation of either the NGI or ACI is not likely to incur significant bias associated with the assumption of ideal stage collection efficiency profiles, except perhaps for abbreviated ACI systems where the incoming aerosol is nearer to monodisperse (GSD, ≤1.2) than is likely with OIP-generated aerosols.

REFERENCES

1. Marple VA, Willeke K. Inertial impactors: theory, design and use. In: Liu BYH, editor. Fine particles. New York: Academic; 1976. p. 411–66.
2. Heyder J, Svartengren MU. Basic principles of particle behavior in the human respiratory tract. In: Bisgaard H, O'Callaghan C, Smaldone GC, editors. Drug delivery to the lung. New York: Marcel Dekker; 2002. p. 21–45.
3. Mitchell JP, Nagel MW. Cascade impactors for the size characterization of aerosols from medical inhalers; their uses and limitations. J Aerosol Med. 2003;16:341–76.
4. European Directorate for Quality in Medicines and HealthCare (EDQM). Monograph 2.9.18: European Pharmacopeia, Preparations for inhalation: aerodynamic assessment of fine particles. 67075 Strasbourg, France: Council of Europe; 2012. Ph.Eur. 7.5.
5. United States Pharmacopeia. Chapter 601: aerosols, nasal sprays, metered-dose inhalers and dry powder inhalers. Rockville, MD, USA: United States Pharmacopeial Convention; 2012. USP 35-NF 30.
6. European Medicines Agency (EMA). Guideline on the pharmaceutical quality of inhalation and nasal products. London, UK: 2006. EMEA/CHMP/QWP/49313/2005 Corr. 2006. http://www.ema.europa.eu/docs/en_GB/document_library/Scientific_guideline/2009/09/WC500003568.pdf. Accessed 4 Oct 2012.
7. Health Canada (HC): Guidance for Industry: pharmaceutical quality of inhalation and nasal products, Ottawa, Canada: 2006. Document 06-106624-547. Available at http://www.hc-sc.gc.ca/dhp-mps/prodpharma/applic-demande/guide-ld/chem/inhalationnas-eng.php. Accessed 4 Oct 2012.
8. United States Federal Drug Administration (FDA). Draft guidance: metered dose inhaler (MDI) and dry powder inhaler (DPI) drug products chemistry, manufacturing and controls documentation. Rockville, MD, USA: FDA; 1998. Docket 98D-0997. Available at http://www.fda.gov/downloads/Drugs/…/Guidances/ucm070573.pdf. Accessed 4 Oct 2012.
9. Marple VA, Liu BYH. Characteristics of laminar jet impactors. Environ Sci Technol. 1974;8(7):648–54.
10. Marple VA, Rubow KL, Olson BA. Inertial, gravitational, centrifugal, and thermal collection techniques. In: Baron PA, Willeke K, editors. Aerosol measurement: principles, techniques and applications. 2nd ed. New York: Wiley; 2001. p. 229–60.
11. O'Shaughnessy PT, Raabe OG. A comparison of cascade impactor data reduction methods. Aerosol Sci Tech. 2003;37(2):187–200.

12. Rader DJ, Mondy LA, Brockmann JE, Lucero DA, Rubow KL. Stage response calibration of the Mark III and Marple personal cascade impactors. Aerosol Sci Tech. 1991;14(3):365–79.
13. Dunbar C, Mitchell J. Analysis of cascade impactor mass distributions. J Aerosol Med. 2005;18(4):439–51.
14. Vaughan NP. The Andersen impactor: calibration, wall losses and numerical simulation. J Aerosol Sci. 1989;20(1):67–90.
15. Marple VA, Roberts DL, Romay FJ, Miller NC, Truman KG, Van Oort M, *et al*. Next generation pharmaceutical impactor (a new impactor for pharmaceutical inhaler testing). Part I: Design. J Aerosol Med. 2003;16(3):283–99.
16. Mitchell JP, Tougas T, Christopher JD, Lyapustina S, Glaab W. The abbreviated impactor measurement and efficient data analysis concepts: Why use them and when. In: Byron PR, Peart J, Suman JD, Farr SJ, editors. Respiratory drug delivery 2012. River Grove: Davis Healthcare International Publishing; 2012. p. 731–5.
17. Mitchell JP. Good practices of qualifying cascade impactors (CIs): a survey of members of the European Pharmaceutical Aerosol Group (EPAG). Drug Delivery to the Lungs-16. Edinburgh: The Aerosol Society; 2005. p. 189–92.
18. Nichols SC, Mitchell JP. Impactor Use Survey 2012: An Industry Perspective on behalf of the European Pharmaceutical Aerosol Group (EPAG), Drug Delivery to the Lungs-23. Edinburgh, UK: The Aerosol Society; 2012. p. 216–9.
19. Christopher D, Dey M, Lyapustina S, Mitchell J, Stein S, Tougas T, *et al*. Generalized simplified approaches for MMAD determination. Pharm Forum. 2010;36(2):812–23.
20. Thiel CG. Cascade impactor data and the lognormal distribution: nonlinear regression for a better fit. J Aerosol Med. 2002;15(4):369–78.
21. Lewis D. CITDAS version 3.0 wibu offers new options for processing cascade impactor deposition data. Inhalation. 2008;2(4):7–10.
22. Hinds WC. Properties, Behavior, and Measurement of Airborne Particles. 2nd ed. New York: Wiley; 1999.
23. Roberts DL. Theory of multi-nozzle impactor stages and the interpretation of stage mensuration data. Aerosol Sci Tech. 2009;43(11):1119–29.
24. Marple VA, Olson BA, Santhanakrishnan K, Mitchell JP, Murray SC, Hudson-Curtis BL. Next generation pharmaceutical impactor, part ii: archival calibration. J Aerosol Med. 2003;16(3):301–24.
25. Marple VA, Olson BA, Santhanakrishnan K, Mitchell JP, Murray SC, Hudson-Curtis BL. Next generation pharmaceutical impactor, part iii: extension of archival calibration to 15 L/min. J Aerosol Med. 2004;17(3):335–43.
26. Gulak Y, Jayjock E, Muzzio F, Bauer A, McGlynn P. Inversion of Andersen cascade impactor data using the maximum entropy method. Aerosol Sci Tech. 2010;44(1):29–37.
27. Mathews J, Walker RL. Mathematical methods of physics. Benjamin WA editor, 2nd Edition. Menlo Park, CA: Benjamin/Cummings; 1970. p 77.
28. Svensson M, Berg E. Measuring the fine particle dose using interstage filters in the NGI: an overview of two methods. AIM Specialty Workshop at Drug Delivery to the Lung 21. Edinburgh, UK: The Aerosol Society; 2010. p. 382–5.
29. Mitchell JP, Nagel MW, Avvakoumova V, MacKay H, Ali R. The abbreviated impactor measurement (AIM) concept: part 1—influence of particle bounce and re-entrainment—evaluation with a "dry" pressurized metered dose inhaler (pMDI)-based formulation. AAPS PharmSciTech. 2009;10(1):243–51.
30. Mitchell JP, Nagel MW, Avvakoumova V, MacKay H, Ali R. The abbreviated impactor measurement (AIM) concept: part 2—influence of evaporation of a volatile component—evaluation with a "droplet producing" pressurized metered dose inhaler (pMDI)-based formulation containing ethanol as co-solvent. AAPS PharmSciTech. 2009;10(1):252–7.
31. Mathews J, Walker RL. Mathematical methods of physics. Benjamin WA editor, 2nd Edition. Menlo Park, CA: Benjamin/Cummings; 1970. p. 351.
32. Fuchs NA, Sutugin AG. Generation and use of monodisperse aerosols. In: Davies CN, editor. Aerosol science. New York: Academic; 1966. p. 1–30.
33. Cripps A, Riebe M, Schulze M, Woodhouse R. Pharmaceutical transition to non-CFC pressurized metered dose inhalers. Respir Med. 2000;94(Supple. B):3–9.
34. Rudolph G, Köbrich R, Stahlhofen W. Modeling and algebraic formulation of regional aerosol deposition in man. J Aerosol Sci. 1990;21(Supple. 1):403–6.
35. Mitchell JP, Newman S, Chan HK. *In Vitro* and *In Vivo* Aspects of Cascade Impactor Tests and Inhaler Performance: A Review. AAPS PharmSciTech. 2007;8(4):article 110. doi: 10.1208/pt0804110.
36. Leach CT. Enhanced drug delivery through reformulating MDIs with HFA propellants: drug deposition and its effect on preclinical and clinical programs. In: Dalby RN, Byron PR, Farr SJ, editors. Respiratory drug delivery-V. Buffalo Grove: Interpharm Press Inc; 1996. p. 133–44.
37. Labiris NR. Dolovich MB pulmonary drug delivery. Part I: physiological factors affecting therapeutic effectiveness of aerosolized medications. Br J Clin Pharmacol. 2003;5(12):588–99.
38. Bonam M, Christopher D, Cipolla D, Donovan B, Goodwin D, Holmes S, *et al*. Minimizing variability of cascade impaction measurements in inhalers and nebulizers. AAPS Pharm Sci Tech. 2008;9(2):404–13.